Robust Gait Recognition by Integrating Inertial and RGBD Sensors

Qin Zou, *Member, IEEE*, Lihao Ni, Qian Wang, *Member, IEEE*, Qingquan Li, and Song Wang, *Senior Member, IEEE*

***Abstract*—Gait has been considered as a promising and unique biometric for person identification. Traditionally, gait data are collected using either color sensors, such as a CCD camera, depth sensors, such as a Microsoft Kinect, or inertial sensors, such as an accelerometer. However, a single type of sensors may only capture part of the dynamic gait features and make the gait recognition sensitive to complex covariate conditions, leading to fragile gait-based person identification systems. In this paper, we propose to combine all three types of sensors for gait data collection and gait recognition, which can be used for important identification applications, such as identity recognition to access a restricted building or area. We propose two new algorithms, namely EigenGait and TrajGait, to extract gait features from the inertial data and the RGBD (color and depth) data, respectively. Specifically, EigenGait extracts general gait dynamics from the accelerometer readings in the eigenspace and TrajGait extracts more detailed subdynamics by analyzing 3-D dense trajectories. Finally, both extracted features are fed into a supervised classifier for gait recognition and person identification. Experiments on 50 subjects, with comparisons to several other state-of-the-art gait-recognition approaches, show that the proposed approach can achieve higher recognition accuracy and robustness.**

***Index Terms*—Accelerometer, dense trajectories, gait recognition, multisensor integration, person identification.**

I. Introduction

USING gait for person identification has been drawing more and more attention in recent years [1]–[3], due to its capability in identifying a person at a longer distance than the traditional biometrics based on face, fingerprint or iris recognition. However, in practice, gait biometrics usually suffer from two issues. First, the data collected by a single type of sensors, e.g., a CCD camera, may only capture part of the gait features and this may limit the gait recognition accuracy. Second, gait biometrics are usually sensitive to hard-covariate conditions, e.g., walking with hands in pocket or with loadings. In this paper, we propose to combine gait data collected by different types of sensors to promote the gait recognition accuracy and the robustness.

In the previous research, there are mainly three types of sensors that have been used for gait data collection and gait recognition—color sensors, depth sensors, and inertial sensors. Using color sensors, e.g., CCD cameras, a walking person can be captured into a video, in which each frame is a 2-D RGB (color) image of the person and the surrounding environment. Gait recognition on such a video is usually achieved by segmenting, tracking, and analyzing the silhouette of the walking person on each frame [4]–[11]. The silhouette segmentation and tracking can be difficult when the color of the person is similar to the color of the surrounding environment in the video. In addition, color sensors generally capture the dynamic gait features in a 2-D space.

Using depth sensors, such as the line-structure light devices, it is usually easier to segment a walking person from the surrounding environment, when there is no other moving objects around. In addition, from the depth data, 3-D dynamic gait features can be derived for gait recognition [12]–[14]. However, in practice depth data may contain noise and errors, especially at the spots with strong reflectiveness, e.g., on a reflective clothing, where the depth value is totally invalid. Such errors may lead to incorrect gait features and gait recognition results.

Different from color and depth sensors, which are installed to capture the walking person at a distance to collect gait data, inertial sensors such as accelerometers and gyroscopes collect gait data by attaching to and moving with the person [15]–[21]. The inertial sensor-based gait recognition mainly benefits from the extensive use of smartphones—people always carry their smartphones and almost all the smartphones have integrated inertial sensors of accelerometers and gyroscopes. Considering the usability, the smartphone must be allowed to be placed in any pockets with different orientations when we use its inertial sensors for gait recognition. Such different placements and orientations of the sensors may vary the inertial data and affect the gait recognition accuracy [18].

In general, each type of the above-mentioned sensors can capture part of the gait features with different kinds of errors and incompleteness. For example, depth and inertial sensors

Manuscript received December 16, 2016; accepted March 10, 2017. Date of publication March 29, 2017; date of current version March 15, 2018. This work was supported in part by the National Natural Science Foundation of China under Grant 61301277, Grant 61672376, Grant 61373167, Grant U1636219, Grant 41371377, and Grant 91546106, in part by the Open Research Fund of State Key Laboratory of Information Engineering in Surveying, Mapping and Remote Sensing under Grant 16S01, and in part by the National Basic Research Program of China under Grant 2012CB725303. This paper was recommended by Associate Editor J. Su. *(Corresponding author: Qian Wang).*

Q. Zou, L. Ni, and Q. Wang are with the State Key Laboratory of Software Engineering, School of Computer Science, Wuhan University, Wuhan 430072, China (e-mail: qzou@whu.edu.cn; lhni@whu.edu.cn; qianwang@whu.edu.cn).

Q. Li is with the Shenzhen Key Laboratory of Spatial Smart Sensing and Service, Shenzhen University, Shenzhen, China (e-mail: liqq@szu.edu.cn).

S. Wang is with the Department of Computer Science and Engineering, University of South Carolina, Columbia, SC 29200 USA (e-mail: songwang@cec.sc.edu).

Color versions of one or more of the figures in this paper are available online at http://ieeexplore.ieee.org.

Digital Object Identifier 10.1109/TCYB.2017.2682280

capture 3-D gait features and color sensors capture 2-D gait features. Meanwhile, the inertial data, such as the accelerometer readings, portrait the motion pattern of the whole body and provide a general description to the gait dynamics, while the color and depth data can be used to infer the motion of many body parts and provide more detailed subdynamics of the gait. It is natural to assume that the gait features derived from different sensors can complement each other. This motivates the proposed approach to integrate the color, depth, and inertial sensors for more accurate gait recognition.

Sensitivity to complex covariate conditions is another main issue in gait biometrics [6]. For example, gait data from a sensor may look different when the same person walks with hands in pocket or with loadings. Such a difference increases the variance of a person's gait features and reduces the gait recognition accuracy. In this paper, through carefully designed experiments, we show that the proposed approach of integrating different sensors can also improve the robustness of gait recognition under complex covariate conditions.

As a practical application scenario, the proposed approach of integrating different sensors for gait recognition can be used for person identification to access a restricted area or building. As illustrated in Fig. 1, at the entrance of a restricted area, a user simply walks on a force platform to get his identity verified. During his walk, a preinstalled client application in his smartphone sends real-time inertial-sensor readings to the server by wireless communication. At the same time, color and depth sensors, mounted over the ceiling and facing the platform, collect the RGBD (color and depth) data and send them to the server. In the server, the proposed approach can integrate all the data and perform gait recognition to identify whether he is an authorized user or not. Other than a higher gait recognition accuracy, such an identification system also has good security—even if the smartphone is hacked to send forged inertial data to the server, it is difficult to forge the RGBD data since color and depth sensors are not controlled by the user.

Following the scheme of identification illustrated in Fig. 1, in this paper we use accelerometer in the smartphone to collect inertial data and Microsoft Kinect to collect the color and depth data. We develop a new EigenGait algorithm to capture the general gait dynamics by analyzing the inertial data in the eigenspace and a new TrajGait algorithm to capture more detailed gait subdynamics based on the 3-D trajectories extracted from the RGBD video. The extracted features on general dynamics and subdynamics of gait are then integrated and fed into a supervised classifier for gait recognition and person identification. In the experiments, we collect three sets of inertial and RGBD data from 50 subjects and evaluate the proposed approach under various covariate conditions. Comparison results with other approaches confirm that the gait recognition accuracy and robustness can be improved by integrating different types of sensors. The main contributions of this paper lie in threefold.

1) For the problem that sensors of the same type, e.g., only using color sensors, are incapable of capturing adequate gait information for person identification, a multisensor integration method is proposed for gait recognition, in which the inertial sensor is utilized to capture general dynamics of gait, and the color sensor and depth sensor are used to capture detailed subdynamics of gait. The multisensor data fusion leads to more robust gait-recognition performance.
2) For the problem that sparse points, e.g., skeleton points, on human body have limitations in describing gait features, a novel 3-D dense trajectory algorithm is proposed to describe the detailed subdynamics of gait by using the RGBD videos, where dense points are tracked on the RGB channel and are assigned with spatial information by the depth channel of the RGBD video. To the best of our knowledge, it is the first to create 3-D dense trajectories and use them for gait recognition. We find that such gait features are more discriminative than the skeleton- or joints-based features in gait recognition.
3) Three new datasets, with both RGBD and accelerometer data, are collected on 50 subjects. They can be used for quantitative evaluation and performance comparison of different gait recognition methods.

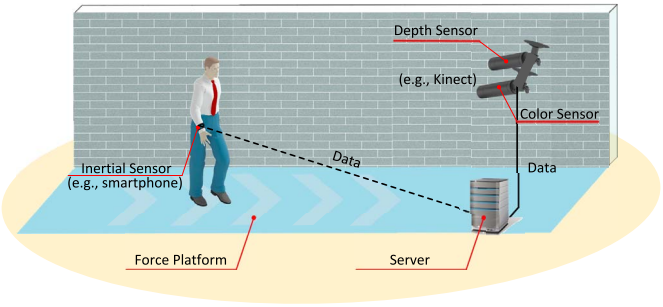

Fig. 1. Application scenario of the proposed approach: a gait-based person identification system for accessing a restricted area.

The remainder of this paper is organized as follows. Section II reviews the related work. Section III introduces the proposed approach, including sensor setting, data collection, gait feature extraction, and integrated gait recognition. Section IV reports the experiments and results. Section V concludes this paper and briefly discusses the possible future work.

II. Related Work

The ideas and experiments of gait recognition can be traced back to Cutting and Kozlowski's [22] work, in which the manner of walking, i.e., the gait, was found to be possible to identify a person. Since then, gait-based person identification has attracted extensive attention in both academia and industry [23], and a number of gait recognition methods have been proposed. In these methods, three types of sensors are mainly used for gait data collection, namely the color sensor, the depth sensor, and the inertial sensor. Hence, the gait recognition methods can be classified into the color-based, the depth-based, and the inertia-based. In this section, we briefly overview them, as well as a brief overview to other action-based biometrics.

A. Color-Based Methods

The color-based methods had a rapid development in the early days [4]–[6], [24]–[31]. These methods can be classified

into the model-free methods and the model-based methods. In the model-free methods, gait features are often extracted by analyzing the shapes, or contours, of the silhouettes in successive frames. In addition, features on the velocity, texture and color are also examined. One important work among them is the gait energy image (GEI) method [5], which represents gait dynamics by an aligned and normalized silhouettes over a gait cycle. The GEI provides a compact representation of the spatial occupancy of a person over a gait cycle. However, partitioning gait cycles from a color video is rarely easy. In [25] and [32], silhouettes were produced by background subtraction, and gait features were extracted by principal component analysis (PCA). In [33] and [34], statistic methods were employed to analyze the gait characteristics on a sequence of binary silhouettes images. Motion has been exploited for gait representation [35]–[37]. In [35], motion is described by local binary patterns, and hidden Markov model is then applied to distinguish the gait dynamics of different persons. In [38], gait motions were encoded based on a set of spatio-temporal interest points from a raw gait video. These interest points were detected by using Harris corner detector from the regions with significant movements of human body in local video volumes. In [36], motions were computed based on a sequence of silhouette images. In [37], motions were computed on multi-view color videos, and the trajectories were encoded by Fisher vectors for gait representation. The model-based approaches commonly use *a priori* model to match the data extracted from a video [39], [40], and parameters of the model are then used for gait recognition. For example, in [40], a pendulum model is used to describe the leg movement of the body.

Similar to [37], in this paper, we also extract gait features from trajectories. However, we develop a new algorithm that is totally different from [37], with availability of other sensors and a goal to extract more accurate gait dynamics. First, we segment the walking person from the background by using a depth sensor. This way, we can more accurately and reliably extract the human silhouette than many human detection algorithms [41] which only generate rectangular bounding boxes around the person. Second, we compute dense trajectories other than sparse interest points and the use of dense trajectories can encode more detailed gait dynamics.

B. Depth-Based Methods

With the development of depth sensors, e.g., Microsoft Kinect, it is easier to segment human body from the background and many depth-based gait recognition methods have been proposed recently [12], [14], [42]–[44]. Under the assumption that body movements can be described by the trajectories of body joints, Munsell *et al.* [42] proposed a full-body motion-based method for person identification. It examines the motion of skeletons, i.e., a number of joints tracked by the Kinect, and constructs a position matrix based on the location of the joints. All the position matrices are then dealt with by an singular value decomposition (SVD) operation for feature extraction. Following the idea of GEI, Sivapalan *et al*. [12] proposed the use of gait energy volume (GEV) to represent gait dynamics with a sequence of GEIs, in which reasonably good recognition accuracy can be achieved based only on the frontal depth information of gait. However, these depth-based methods characterize the gait dynamics only using the depth information and neglect more detailed gait dynamics implied in the human appearance. In [14], pose depth volume (PDV) was used to improve GEV by extracting accurate human silhouettes, in which color information is used to improve the segmentation of human mask from the depth video. But PDV does not use color information for gait representation. In [45], depth features on body joints were obtained from Kinect depth camera, and the GEI features were extracted from color images. The combined RGBD features were then used for frontal gait recognition. Different from [45], the proposed method uses color images to compute the 2-D dense trajectories, which are then combined to the depth data to build dense 3-D trajectories for extracting more detailed gait subdynamics.

C. Inertia-Based Methods

Early researches on inertia-based gait recognition can be found in [15] and [16]. In [15], a portable tri-axial accelerometer device is used, and the gait is represented by the correlation of acceleration curves and the distribution of acceleration signals in the frequency domain. In [16], a template matching strategy is used for gait-based person identification, in which the acceleration signals are divided by gait cycles, and then dynamic time warping is applied to check the similarity of two gait curves. In [46] and [47], gait cycles were detected and cycle matching were performed to improve the accuracy of gait recognition in the context of authentication or identification. In recent years, smartphones equipped with accelerometer and gyroscope have been widely used, which makes it easier and cheaper to conduct an inertia-based gait recognition [17], [18], [21], [48]. In [18], a Mexican hat wavelet transform is applied to the acceleration data to analyze the gait patterns, and most discriminative features are selected based on a Fisher-ratio value. In [49], large-scale data were collected for gait recognition, in which the accelerometer is fixed on the human body. In [50], to avoid the complications in gait-cycle detection, signature-meaningful points (SPs) on the acceleration curve were detected, and gait features extracted on SPs were used for gait recognition. In [21], the gyroscope is used to rectify the orientation of the accelerometer. The acceleration signals with orientations are calculated with auto-correlation and converted into the frequency domain using fast Fourier transformation (FFT). However, the gyroscope commonly has a cumulative-error problem, which may lead to an unreliable rectification and the difficulty in determining the similarity of two gait curves. Another limitation is that the detection accuracy of previous approaches highly relies on the very accurate placement of the accelerometer sensor on the human body. This strict requirement would greatly affect the usability and flexibility of the identification system.

D. Other Action-Based Biometrics

Also related to this paper is the action- or activity-based person identification [51]–[59]. Besides gait, many other actions

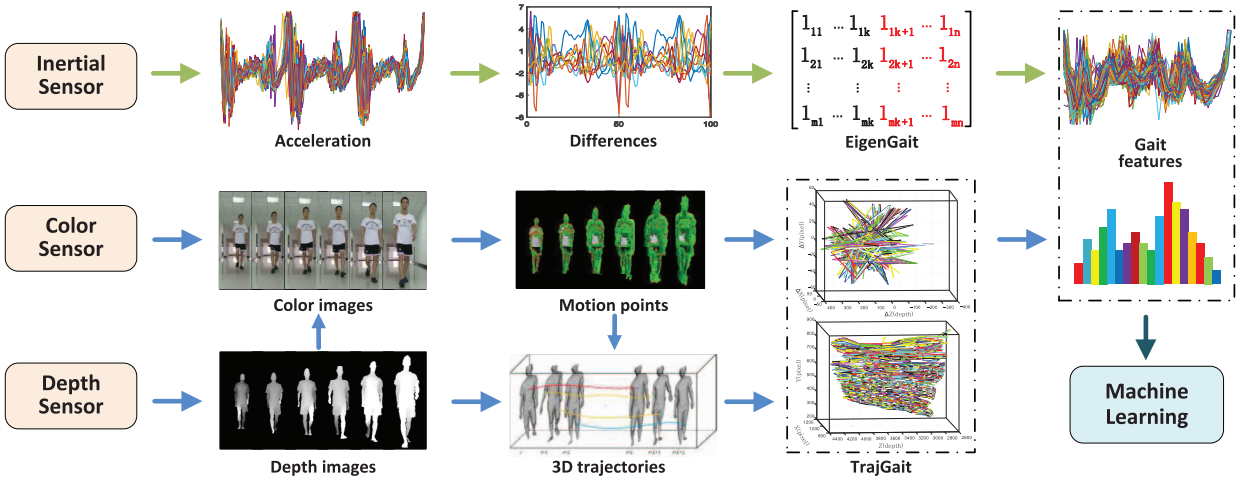

Fig. 2. Flowchart of the proposed gait-based person identification system.

such as jump, run and skip are also found to be capable of identifying a person. Kobayashi and Otsu [51] proposed to identify persons from a sequence of motion images using an auto-correlation-based method. By incorporating more types of human actions, Gkalelis *et al*. [52] presented a multimodal method for person identification, and enhanced it by using a multicamera setup to capture the human body from different viewing angles [53]. Recently, sparse-coding-based methods were developed for human identification based on the activities captured by videos [55]–[57]. In [55], a metric learning procedure was performed on the sparse-coded features to get discriminative features. In [56] and [57], the discriminative power was further improved by performing a discriminative sparse projection and learning a low-dimensional subspace for feature quantization. In [58], multiple Kinects were found to improve the performance of gesture-based authentication. In [59], a generative model was presented to describe the action instance creation process and an MAP-based classifier was used for identity inference on 3-D skeletal datasets captured by Kinect.

III. Proposed Method

A. System Overview

Following the application scenario of person identification shown in Fig. 1, we let the user walk straight along a corridor for gait feature collection. The inertial sensors are with the user while the color and depth sensors are placed at the end of the corridor. In this paper, we use accelerometer in the smartphone as inertial sensors and Microsoft Kinect as color and depth sensors. This way, we collect the accelerometer readings and RGBD data for gait feature extraction and gait recognition. Note that, the color (RGB) data and depth data collected by Kinect are temporally synchronized.

The flowchart of the proposed system is illustrated in Fig. 2. After data preprocessing, gait features are then extracted from the inertial data and RGBD data by using the proposed EigenGait and TrajGait algorithms, respectively. Finally, the gait features are combined as an input to the machine learning component for person identification. The proposed system can be installed at the entrance of any restricted area for person identification, such as banks, financial tower, military base, etc.

The proposed gait recognition combining multiple sensors is not fully noninvasive. The inertial sensors move with the user and send the accelerometer data to the server. Therefore, the user should be notified in prior and may need to show certain level of cooperation in data collection. But from the application perspective, most, if not all, existing person-identification systems for accessing a restricted area cannot be fully noninvasive—many of them work as a verification system where the user needs to provide his identity to the server for verification at the entrance. For such a person-identification system, the goal is to achieve good usability instead of full noninvasiveness. For better usability, a person-identification system should require as fewer human interactions and less strict cooperations as possible. For the proposed system, with appropriate settings and client applications in each user's smartphone, the data collection, including sending the inertial and RGBD data, and possibly the user's identity, to the server, and the whole process are fully automatic without additional human interactions. In addition, as shown in the later experiments, by combining multiple sensors, the proposed system shows higher robustness against covariate conditions. This also improves the usability by requiring less strict cooperations from the user.

In the following, we first introduce the data collection and data preprocessing, and then elaborate on the EigenGait algorithm for inertia-based gait representation and the TrajGait algorithms for color- and depth-based gait representation.

B. Data Collection and Preprocessing

In this paper, we use accelerometer to collect inertial data and Kinect to collect RGBD data.

1) Acceleration Data: We utilize a tri-axial accelerometer sensor in the smartphone to collect the acceleration data of a walking person. First, we build an application on the Android platform. Given the APIs provided by the Android SDK, we use the *android.harware.SensorManager* package

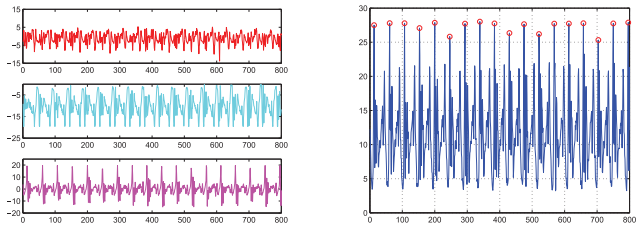

(a) (b)

Fig. 3. Example of the acceleration data and its partitions. (a) Acceleration values Acc_x, Acc_y, and Acc_z on the x, y, and z axes, respectively. (b) Compound acceleration values Acc_c, and the partitioning points (as marked by red circles).

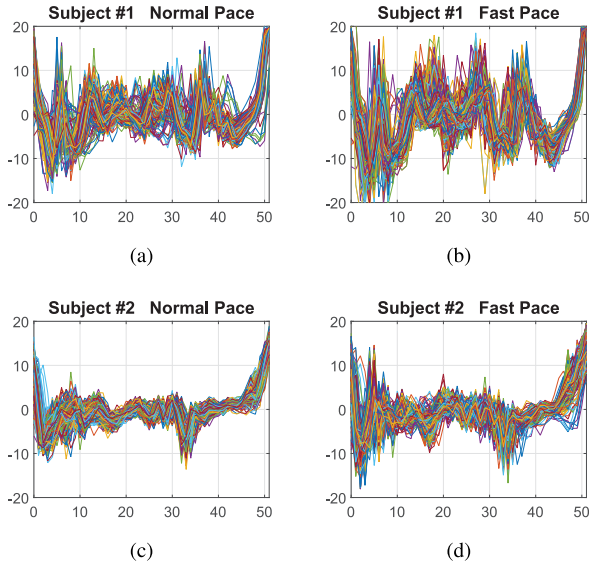

(a) (b) (c) (d)

Fig. 4. Comparison of acceleration curves collected by different subjects and on different walking paces. Acceleration curves of (a) and (b) user #1 in normal pace and fast pace, respectively, and (c) and (d) user #2 in normal pace and fast pace, respectively.

and attached event listeners to the *Sensor.Type_Accelerometer* to collect acceleration data. The sensor is registered to the *SensorManager.Sensor_Delay_Game* and is set a sampling rate of 50 Hz on each axis.

Considering the usability, in data collection we simply ask the user to put the smartphone, installed with our application, in his/her pocket with any orientation. Each user is required to walk in his/her normal pace and fast pace. Since the accelerometer is placed in the pocket with a random orientation, which varies over time during the walking, the acceleration values on each axis are collected in a time-varying direction. Therefore, the acceleration values along each axis are actually not comparable from time to time. To address this issue, we fuse the acceleration values on all three axes into one compound one. Let Acc_x, Acc_y, and Acc_z be the acceleration values on the x, y, and z axes, respectively, we compute the compound acceleration value Acc_c by $\text{Acc}_c = \sqrt{\text{Acc}_x^2 + \text{Acc}_y^2 + \text{Acc}_z^2}$, which is more robust against the pose change of the accelerometer over time.

Fig. 3(a) shows an acceleration data sample on the x, y, and z axes collected by a smartphone—the periodical property

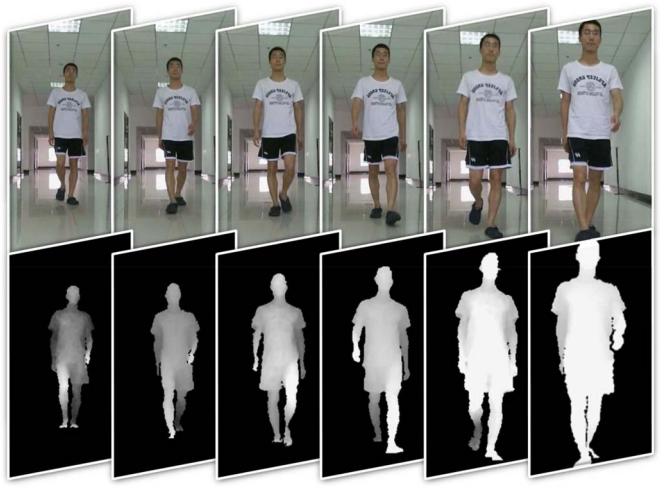

Fig. 5. Color and depth data collected by Kinect. Top row: a sequence of RGB images show a person walking toward the sensors. Bottom row: the corresponding depth images. Note that, to give a better display, we crop the images by only showing the region around the person.

of the acceleration data reflects the walking pace of the user. Fig. 3(b) shows the compound acceleration curve, which has been partitioned at local maximum. Specifically, we sequentially consider a point as the partitioning point if it satisfies three conditions.

1) It is a local maximum (peak) along the curve.
2) Its distance to the previous partitioning point is no less than 700 ms.
3) Its value is greater than 4 m/s^2.

Each segment of the partitioning acceleration curve corresponds to one step in the walking. Note that, in this paper, one step denotes a full step cycle consisting of a left-foot move and a right-foot move. Fig. 4(a) and (b) shows 100 one-step acceleration-curve segments of a user, under normal pace and fast pace, respectively, and Fig. 4(c) and (d) shows those of another user. We can see that, although the acceleration curves vary a lot between different users, the acceleration curves of the same user share similar shapes, even under different paces.

2) Color and Depth Data: A Kinect 2.0 assisted with Kinect SDK v2.0[1] is applied for color and depth data collection. The Kinect is placed about 0.5 m up from the ground. The RGB video stream is in 24-bit true color format with a resolution of 1280×1024 pixels. The depth video stream is in VGA resolution of 640×480 pixels, with 13-bit depth value. The depth sensor has a practical ranging limit of 1.2–3.5 m distance when using the Kinect SDK. The sampling rate is 15 frames/s. Fig. 5 shows a sequence of color images and depth images collected by the Kinect. The depth images shown in Fig. 5 have been normalized since a single VGA channel has only 8 bits to represent a pixel. For the computation in all the experiments, the original 13-bit depth value is used, which provides a high precision to describe the motion in the depth channel.

[1]http://www.microsoft.com/en-us/kinectforwindows/develop/downloads-docs.aspx

Fig. 6. Data collection under eight different hard-covariate conditions.

3) Three Datasets: Using the sensor settings as described above, we collect three datasets consisting of both RGBD data and accelerometer readings. We use these data for evaluating the performance of the proposed method, as well as the comparison methods, in the later experiments.

1) *Dataset #1:* This dataset is collected on ten subjects, containing 1000 groups of acceleration data and 1000 groups of RGBD data—100 groups of acceleration data and 100 groups of RGBD data are collected for each subject, with half in normal pace, and half in fast pace. The acceleration data and RGBD data are collected separately. In collecting acceleration data, each subject is required to walk along a hallway, with a length of about 60 ft. *A group of acceleration data* is defined as the sequence of acceleration values resulting from the entire walk from one end of the hallway to the other end. We partition the acceleration data into steps as illustrated in Fig. 3(b). For all the one-step acceleration data, we temporally interpolate them into a data sequence of length 50. Based on the temporally partitioning, we create five subdatasets, containing one-, two-, three-, four-, and five-step long data samples, respectively. In RGBD data collection, each subject is required to walk toward the Kinect 100 times, from about 5 m away to 1 m away to the Kinect. The sequences of frontal color and depth images of the subjects are captured. *A group of RGBD data* is defined as the sequence of RGBD images resulting from one full walk toward the Kinect.
2) *Dataset #2:* This dataset contains 500 data samples of 50 subjects, with ten data samples for each subject. Each *data sample* consists of a sequence of acceleration data and a sequence of RGBD data, which are collected simultaneously for one full walk of a user. For each RGBD video, a frame is preserved only if the present person is recognized with all the body joints by the Kinect SDK. Each acceleration data covers about two steps or more. We uniformly partition each acceleration data and generate a two-step data sample.
3) *Dataset #3:* This dataset contains 2400 data samples of 50 subjects, with 48 data samples for each subject. These data are collected under different covariate conditions. In particular, in collecting dataset #3, each subject is required to walk under eight different conditions, i.e., natural walking, left hand in pocket, right hand in pocket, both hands in pocket, left hand holding a book, right hand holding a book, left hand with loadings, and right hand with loadings, as shown in Fig. 6. For each subject, six data samples are collected under each condition, with three in fast pace and three in normal pace. Acceleration data and RGBD data are collected simultaneously in each data sample. The information of the above three datasets is summarized in Table I.

C. EigenGait: Eigenspace Feature Extraction for Gait Representation

PCA is a statistical procedure that uses an orthogonal transformation to convert a set of observations of possibly correlated variables into a set of values of linearly uncorrelated variables called principal components. The resulting vectors are an uncorrelated orthogonal basis set. With such properties, PCA is popularly used for constructing predictive models, e.g., the famous eigenface algorithm [60] for face recognition.

In gait data collection, a sequence of (compound) acceleration values resulting from a walk can be plotted into a 2-D curve, as illustrated in Fig. 4 and we call it a *gait curve* in this paper. Given a set of gait curves of N persons, we intend to find the uncorrelated orthogonal basis for all N persons and utilize them to construct discriminative features. This motivates us to apply PCA on the gait curves, and leads to an EigenGait algorithm for gait recognition.

Let $\mathcal{A} = \{\mathcal{S}_i | i = 1, 2, \ldots, N\}$ be a set of gait curves of N subjects, $\mathcal{S}_i$ denotes the gait curves collected for the ith subject. Treating a gait curve as a vector, we can compute an average gait curve for the ith subject as

$$\hat{\mathcal{S}}_i = \frac{1}{M_i} \sum_{j=1}^{M_i} \mathcal{S}_i^{(j)} \tag{1}$$

where M_i is the total number of gait curves collected for the ith subject, and $\mathcal{S}_i^{(j)}$ is the jth gait curve of the ith subject. Further, the overall average gait curve over all the N subjects can be calculated by

$$\hat{\mathcal{S}} = \frac{1}{N} \sum_{i=1}^{N} \hat{\mathcal{S}}_i. \tag{2}$$

Then, a gait-curve difference can be calculated by

$$\mathcal{O}_i = \hat{\mathcal{S}}_i - \hat{\mathcal{S}}. \tag{3}$$

TABLE I
DESCRIPTION OF THE THREE COLLECTED DATASETS

Dataset name	Number of subjects	Acceleration data	RGBD data	Sub-datasets	Walking pace	Other information
Dataset #1	10 Male/Female: 7/3	1,000 groups Normal/Fast: 1:1	1,000 groups Normal/Fast: 1:1	1-step: 5,000 samples, 2-steps: 5,000 samples, 3-steps: 5,000 samples, 4-steps: 5,000 samples, 5-steps: 5,000 samples, for acceleration data.	Normal, Fast	Acceleration data and RGBD data are collected independently.
Dataset #2	50 Male/Female: 39/11	500 samples	500 samples	2-steps: 500 samples	Normal	Acceleration data and RGBD data are collected at the same time.
Dataset #3	50 Male/Female: 39/11	2,400 samples Normal/Fast: 1:1	2,400 samples Normal/Fast: 1:1	2-steps: 2,400 samples	Normal, Fast	Acceleration data and RGBD data are collected at the same time, under 8 covariate conditions.

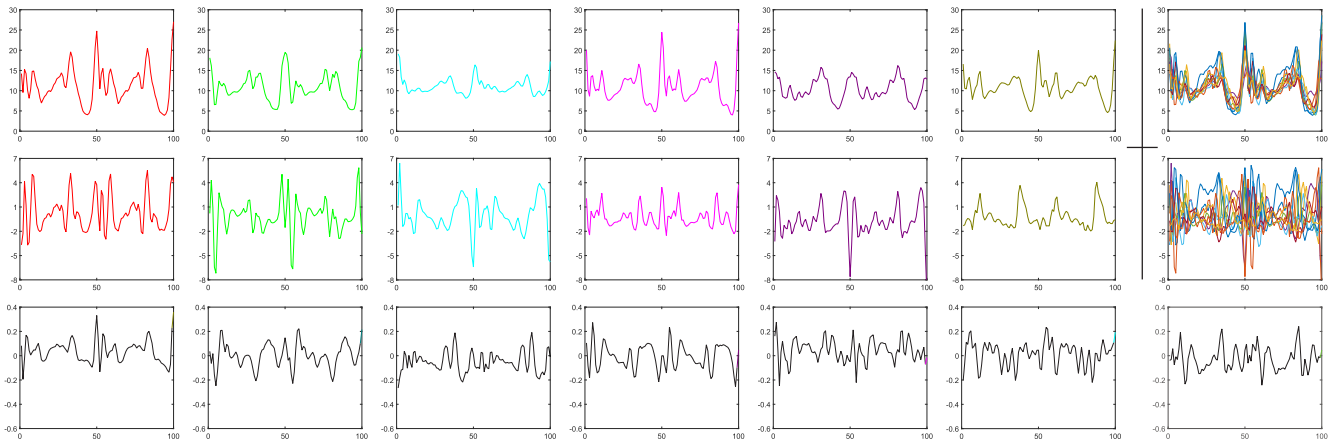

Fig. 7. Example for EigenGaits computation. Top row: the left six figures show the average gait curve ($\hat{\mathcal{S}}_i$) of six subjects in dataset #1, the last one gives an overlay view of the total ten curves. Middle row: the left six show the gait-curve differences ($\mathcal{O}_i$) of the six subjects in the top row, respectively, and the last one gives an overlay view of ten gait-curve differences. Bottom row: from left to right, the top seven eigenvectors (EigenGaits, $\mathcal{U}$) computed on dataset #1.

To better illustrate the meaning of $\mathcal{O}_i$, we compute them on real data. Without loss of generality, let us consider the two-step acceleration data collected in dataset #1. In Fig. 7, the last figure in the middle row shows the gait-curve differences of ten subjects in dataset #1. It can be seen from Fig. 7 that, the gait-curve differences also preserve the periodic property of the original gait curve, as shown in the top row of Fig. 7, and different subjects have different gait-curve differences.

Then the covariance matrix can be calculated by

$$\mathcal{C} = \frac{1}{N}\sum_{i=1}^{N} \mathcal{O}_i \mathcal{O}_i^{\top}. \tag{4}$$

We can perform an eigen-decomposition as

$$(\lambda, \mathcal{U}) = \mathbf{Eigen}(\mathcal{C}) \tag{5}$$

where λ denotes the eigenvalues, and $\mathcal{U}$ denotes the corresponding eigenvectors. Suppose the eigenvalues in λ have been sorted in descending order, we select the first r elements that fulfill $\sum_{i=1}^{r} \lambda_i \geq 0.85 \cdot \sum \lambda$, and hence get r corresponding eigenvectors $\{u_1, u_2, \ldots, u_r\}$. In the bottom row of Fig. 7, the seven curves show the top seven eigenvectors of the two-step subdataset in dataset #1. It can be seen from Fig. 7 that, more distinctiveness can be observed in the gait-curve differences than in the original gait curves. We can also see that, these eigenvectors preserve the shape appearance of some of the original gait curves, as shown in the top row of Fig. 7 and we call them *EigenGaits* in this paper. When a new gait curve s comes, we can project it into the eigenspace defined by the r eigenvectors as

$$\omega_i = u_i^{\top}\left(s - \hat{\mathcal{S}}\right), \quad i = 1, 2, \ldots, r \tag{6}$$

and obtain an EigenGait feature vector $(\omega_1, \omega_2, \ldots, \omega_r)$. As the acceleration data reflects the whole body motion in the walking, the extracted EigenGait features can capture the general gait dynamics.

D. TrajGait: Dense 3-D Trajectories-Based Gait Representation

Before going to details of the algorithm, let us first make some analysis in the perspective of information theory. Following the Shannon's coding theory, the joint entropy of multiple variables, for example two variables X and Y, is defined by:

$$\mathcal{H}(X, Y) = -\sum_{x \in X}\sum_{y \in Y} P(x, y) \log_b P(x, y) \tag{7}$$

(a) (b) (c) (d)

Fig. 8. Example of dense trajectory points extraction. (a) Color image. (b) Corresponding depth image. (c) Segmented mask image. (d) 2-D dense trajectories within the mask, where the red dots indicate the point positions in the current frame. Note that, the image mask has been fine-tuned with image operations, including hole filling, noise removal, and morphological operation.

where $P(x, y)$ is the probability of the state (x, y), b is the logarithm base, which is commonly set as 2, e, or 10. As the entropy of two simultaneous events is no more than the sum of the entropies of each individual event, and are equal if the two events are independent, we have

$$\mathcal{H}(X, Y) \geq \mathcal{H}(X), \mathcal{H}(X, Y) \geq \mathcal{H}(Y). \tag{8}$$

Considering the information in an RGBD video, since the color and depth are independent to each other, we have

$$\mathcal{H}(\text{Color}, \text{Depth}) = \mathcal{H}(\text{Color}) + \mathcal{H}(\text{Depth}) \tag{9}$$

where Color and Depth denote the color channel and depth channel, respectively. Equation (9) inspires us to combine the color and depth information in gait recognition.

In fact, the gait data captured by the color sensor and depth sensor can be represented by a sequence of color images and depth images, respectively. These images provide useful information to describe the details of body movements, e.g., the movement of each body part. We combine the color and depth data and develop a *TrajGait* algorithm for extracting 3-D dense trajectories and describing more detailed gait subdynamics.

TrajGait algorithm is summarized in Algorithm 1, which contains the following four key operations.

1) *computMotion:* One each RGB color frame, we compute the dense optical flow by the algorithm proposed by Farnebäck [61].[2] This algorithm makes a good compromise between accuracy and speed.
2) *segmentMask:* To focus on the walking person, we segment the person from the background, and take it as a mask in later operations. Since the Kinect SDK has provided functions for efficient human detection and joints tracking [62], we apply these functions to extract a raw human mask in each frame, and then apply some image processing techniques, including hole filling and noise removal, to get the final mask. Fig. 8(c) displays a human mask segmented from the depth image in Fig. 8(b). Note that, while segmenting persons from a confusing background can be very challenging on RGBD data, it is not a serious issue in the proposed application scenario of person identification—the environment is highly controlled (e.g., a hallway) and the sensors are well set, without any other moving objects around. In this paper, the following steps are taken to obtain the human mask.
   a) Produce human-oriented depth image using the body-segmentation function provided by Kinect SDK (i.e., IBodyIndexFrame::AccessUnderlyingBuffer).
   b) Resize the depth image to the size of the color image and interpolate the resized image using bicubic interpolation.
   c) Binarize the depth image with a threshold $t = 113$.
   d) Fill the holes and remove segments that are smaller than 1000 pixels.
3) *calcTrajectories:* Suppose (x, y) is the coordinate of a point at a frame of the collected color data, (z) is the depth value of that point in the depth data, then we can locate that point with a coordinate (x_t, y_t, z_t) in the RGBD space. In this way, we can treat each point in the RGBD data as a 3-D point. Fig. 9 illustrates the trajectories in the 3-D space. The shape of a trajectory encodes the local motion patterns, which we use for gait representation. Based on the 2-D dense trajectories extracted by [63] in RGB channels, we can compute the corresponding 3-D trajectories. Let us further suppose point $P_t = (x_t, y_t, z_t)$ at frame t is tracked to frame $t + 1$ at the point P_{t+1}, then, with a given trajectory length L, we can describe its shape by a displacement vector

$$\mathcal{F} = (\Delta P_t, \Delta P_{t+1}, \ldots, \Delta P_{t+L-1}) \tag{10}$$

where $\Delta P_t = (P_{t+1} - P_t) = (x_{t+1} - x_t, y_{t+1} - y_t, z_{t+1} - z_t)$, and L is empirically set as 15. Since the gait may be collected in various walking speed [64], the resulting vector has to be normalized to reduce deviations. As the metric in the color image is different from that in the depth image, we separately normalize them by their sums of the magnitudes of the displacement vectors. We take a normalized displacement vector as a 3-D trajectory descriptor. An example of 3-D trajectory descriptors derived from an RGBD data sequence is shown in Fig. 10.

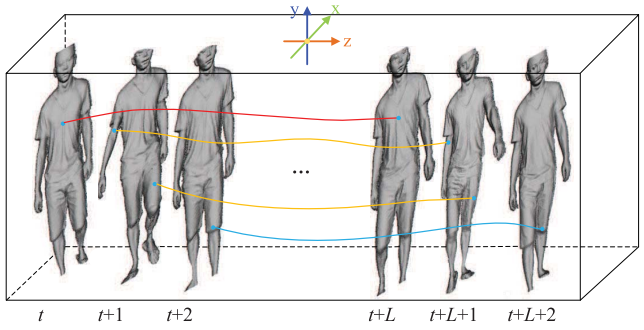

Fig. 9. Illustration of the trajectories in 3-D space.

[2]It is implemented and released by OpenCV 2.4.8 or above.

Algorithm 1 TrajGait Algorithm

procedure TRAJGAIT
  input:
    $V_1, V_2, ..., V_N$: RGB data collected for N subjects,
    $D_1, D_2, ..., D_N$: the corresponding depth data,
    $X_1, X_2, ..., X_N$: the number of data samples in each set,
    $\mathcal{K}$: the number of centers in the K-means clustering,
    L: the number of frames in a trajectory,
  output:
    $\{H_i | i = 1, 2, ..., \mathcal{X}\}$: feature histograms for all RGBD videos, where $\mathcal{X} = \sum_1^N X_i$.
  % Calculate the trajectories of all RGBD data:
  for (i=1 to N) **do**
    for (j=1 to X_i) **do**
      % Compute the motion on the color video $V_i^{(j)}$:
      $\mathcal{M}_i^{(j)} \leftarrow$ **computMotion**$(V_i^{(j)})$;
      % Segment foreground (human) from the depth video:
      $\text{Mask}_i^{(j)} \leftarrow$ **segmentMask**$(D_i^{(j)})$;
      % Calculate 3D trajectories in the RGBD channel:
      $\mathcal{T}_i^{(j)} \leftarrow$ **calcTrajectories**$(\mathcal{M}_i^{(j)}, D_i^{(j)}, \text{Mask}_i^{(j)}, L)$;
      $\mathcal{T}_i \leftarrow$ **putInto**$(\mathcal{T}_i^{(j)})$;
    end for
  end for
  % Put all trajectories together:
  $\mathcal{T} = \{\mathcal{T}_i | i = 1, 2, ..., N\}$;
  % Compute a number of $\mathcal{K}$ centers using Clustering:
  $\mathcal{Y} \leftarrow$ **kMeans**$(\mathcal{T}, \mathcal{K})$;
  % Compute trajectory histogram for each RGBD data sequence:
  for (i=1 to N) **do**
    for (j=1 to X_i) **do**
      $H_i^{(j)} \leftarrow$ **histTrajectory**$(\mathcal{T}_i^{(j)}, \mathcal{Y})$;
    end for
  end for
end procedure

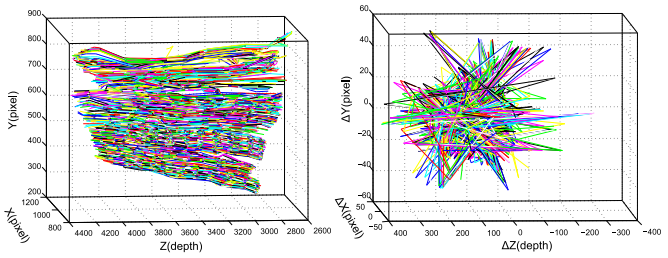

(a) (b)

Fig. 10. Example of the 3-D trajectory descriptors. (a) 3-D trajectories extracted from an RGBD data sequence. (b) 3-D trajectory displacements, i.e., 3-D trajectory descriptors, computed on the trajectories in (a).

4) *histTrajectory:* We apply a bag-of-words strategy to encode the 3-D trajectory descriptors. Specifically, we generate a codebook with a number of K codes using a clustering technique. The standard K-means algorithm is employed here for clustering. To reduce the complexity, we cluster a subset of 1 000 000 randomly selected training samples. To increase the precision, we run K-means 10 times and keep the result with the lowest K-means clustering cost. For each RGBD sequence, the extracted 3-D trajectory descriptors are quantized into a histogram by hard assignment. The resulting trajectory histograms are then used for gait representation.

E. Gait Recognition

We achieve gait recognition using a supervised classifier. We combine the gait features extracted by EigenGait and TrajGait and feed them into a machine learning component for training and testing. The trained model can then be used to recognize new unseen data samples for gait recognition and person identification. For feature combination, we simply concatenate the EigenGait feature and the TrajGait feature into one single feature vector.

In the machine learning component, a multiclass support vector machine (SVM) classifier implemented by libSVM[3] is used for both training and testing [65]. A one-versus-all classification strategy is applied. To investigate the potential relation between classification accuracy and computation efficiency, we try both linear and nonlinear SVMs. For the soft-margin constant C in SVM, we consistently set it 1000 through all the experiments.

IV. Experiments and Results

In this section, we use three datasets to evaluate the performance of the proposed method, as well as the comparison methods. First, we examine the effectiveness of the proposed EigenGait algorithm and the TrajGait algorithm using dataset #1, separately. Then, we evaluate the performance of the proposed method, i.e., the one fusing EigenGait and TrajGait, on dataset #2 by comparing its accuracy with several state-of-the-art gait recognition methods. Finally, we test the robustness of the proposed method on dataset #3. In particular, we try to answer the following questions.

1) How effective are the EigenGait algorithm and the TrajGait algorithm for gait recognition? How do the parameters influence their performances?
2) What is the overall performance of the proposed method? Does it work better than the state-of-the-art color-based methods, depth-based methods, and inertia-based methods?
3) How robust is the proposed method in handling gait data collected under hard-covariate conditions?

In the experiments, we mainly evaluate gait recognition to address a classification problem. At the end of the section, we will also evaluate the proposed method to solve an identification problem. As a classification problem, we use the classification accuracy as a metric for performance evaluation. The classification accuracy is defined as

$$\text{Accuracy} = \frac{\#\text{ Correctly Classified Samples}}{\#\text{ Total Testing Samples}}. \quad (11)$$

In the classification, each testing sample is classified by the pretrained SVM and receives a score vector containing n score values, where n is the number of subjects in training the SVM. A score value in the score vector indicates the likelihood of this sample to be from a specific subject. The sample will be recognized as being from subject i if the ith element is

[3]http://www.csie.ntu.edu.tw/∼cjlin/libsvm/

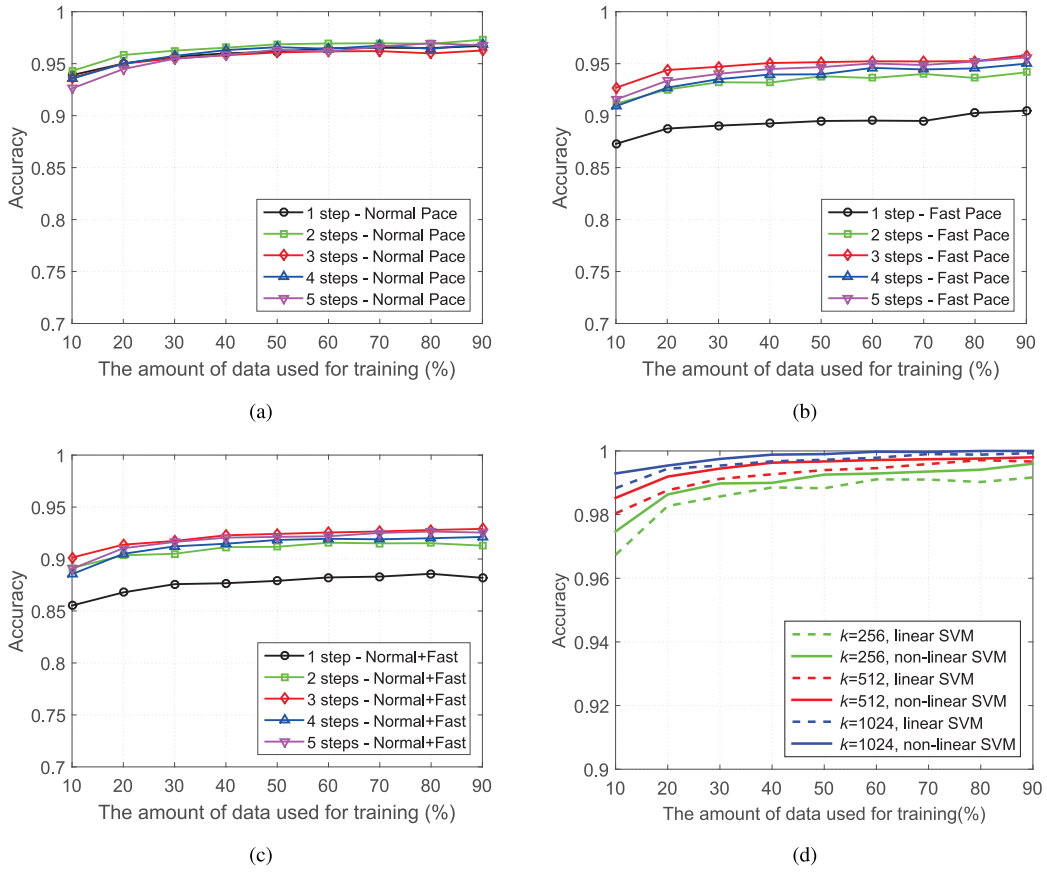

Fig. 11. Performance of the EigenGait and TrajGait. EigenGait on (a) normal pace, (b) fast pace, and (c) normal+fast case. (d) TrajGait on different settings.

the maximum in the score vector. Compared with the ground-truth subject for the test sample, we can decide whether it is correctly classified and compute the accuracy.

A. *Effectiveness*

We use dataset #1 to evaluate the performance of the EigenGait algorithm and the TrajGait algorithm. Dataset #1 is collected for ten subjects, including five subdatasets of the acceleration data, and one subdataset of the RGBD data.

1) EigenGait: There are five acceleration subdatasets, i.e., the one-, two-, three-, four-, and five-step subdatasets. Each subdataset contains 5000 acceleration data sequences, with half in normal pace and half in fast pace. The resulting EigenGait features are of dimension 43, 85, 128, 170, and 213 for the one-, two-, three-, four-, and five-step data, respectively. Note that, data in the same subdataset have no overlaps with each other. The EigenGait algorithm is evaluated under the normal pace, fast pace and two paces mixed, i.e., normal + fast, and the results are shown in Fig. 11(a)–(c), respectively. From Fig. 11(a)–(c), we can see that, EigenGait obtains good classification accuracy in all three cases, e.g., over 0.95 in normal pace, 0.92 in fast pace, and 0.90 in normal+fast, using 30% data for training. Moreover, EigenGait shows higher accuracy under normal pace than under fast pace. This is because a large speed variation would occur when a person walks in a fast pace, which would increase the complexity of the gait data. Decreased performances of EigenGait can be observed in Fig. 11(c), because the mixed-pace data further increase the data complexity.

As can be seen from Fig. 11(b) and (c), on a dataset with large speed variations, e.g., in fast pace, or in normal+fast, EigenGait holds lower performances on the one-step dataset than on two or more step datasets. This is because, a one-step data is less capable of representing the gait than a two or more step data. Surprisingly, the EigenGait obtains comparable performances when varying the data length from 2 to 5 steps. Considering that a two-step data can be easily captured and efficiently computed as comparing to longer data, in our later experiments, we always choose a length of two steps for EigenGait features, including the experiments on datasets #2 and #3.

Further, we evaluate EigenGait's performance using linear and nonlinear SVMs. Typically, the "KL1" and "KCHI2" kernels are employed, respectively. Table II lists the classification accuracy under different walking paces and varied data lengths, where 50% data are used for training. It can be seen that, EigenGait generally shows higher performances using a linear SVM than using a nonlinear one. This is because, the EigenGait extracts gait features in the eigenspace, which makes the feature more linearly classifiable.

2) TrajGait: We use RGBD data in dataset #1 to evaluate the TrajGait algorithm. Specifically, we evaluate the TrajGait under different $\mathcal{K}$ for K-means clustering, and linear and nonlinear SVMs. In K-means clustering, 1000 trajectories are

TABLE II
PERFORMANCE (ACCURACY) OF EIGENGAIT USING LINEAR AND NONLINEAR SVM

Walking pace	Kernel	1 step	2 steps	3 steps	4 steps	5 steps	6 steps	7 steps	8 steps
Normal	KL1	0.9616	0.9616	0.9608	0.9659	0.9634	0.9626	0.9525	0.9606
	KCHI2	0.9522	0.9510	0.9471	0.9520	0.9449	0.9454	0.9393	0.9354
Fast	KL1	0.8948	0.9308	0.9515	0.9398	0.9467	0.9437	0.9387	0.9250
	KCHI2	0.8894	0.9208	0.9433	0.9292	0.9356	0.9244	0.9200	0.9018
Normal&Fast	KL1	0.8790	0.9048	0.9242	0.9183	0.9213	0.9247	0.9094	0.8977
	KCHI2	0.8785	0.8992	0.9156	0.9082	0.9219	0.9054	0.8913	0.8900

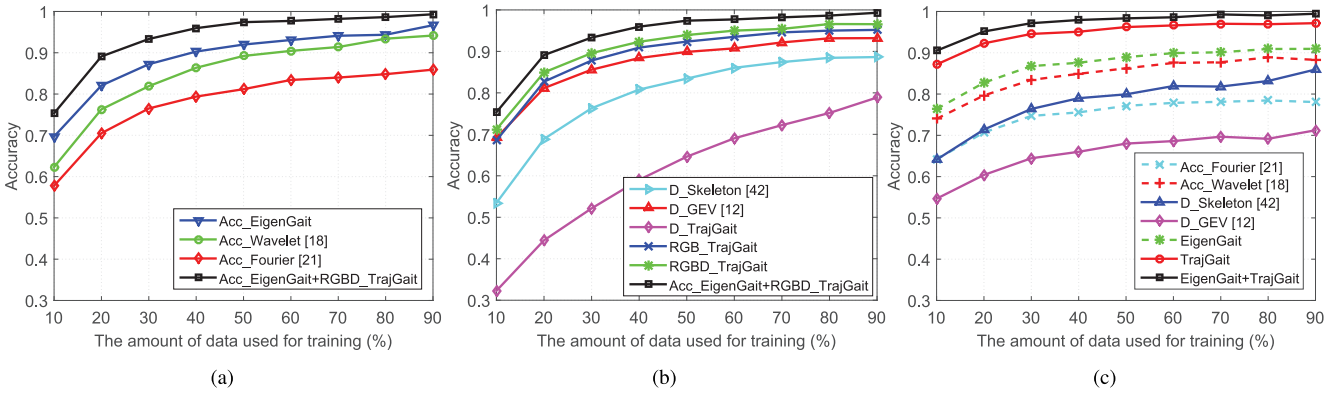

(a) (b) (c)

Fig. 12. Classification performance on datasets #2 and #3. (a) and (b) Performances on dataset #2. (c) Performance on the dataset #3.

randomly selected for each training sample. In feature quantization, all trajectories of each data sample are used, which may span from about 8000–15 000 in our experiments. Fig. 11(d) shows the TrajGait accuracy when $\mathcal{K} = 256$, 512, and 1024, respectively. We can see that the TrajGait achieves classification accuracies higher than 0.98 when using over 20% data for training. A higher performance can be achieved with a larger $\mathcal{K}$, i.e., the codebook size. It can also be observed that, under the same $\mathcal{K}$, a nonlinear SVM produces slightly higher accuracies than the linear one. Considering that linear SVM performs better in EigenGait and has lower computation cost, we choose the linear SVM in the proposed gait recognition by combining the EigenGait and TrajGait features.

B. Accuracy

We evaluate the overall performance of the proposed method, i.e., EigenGait+TrajGait, by comparing it with several other inertia-based methods, color and depth-based methods. Specifically, the following methods are included in the comparison.

1) *Acc_Fourier [21]:* An autocorrelation operation is first applied to the acceleration data, which is then converted into the frequency domain using FFT. The top half of the coefficients are selected as the gait features.
2) *Acc_Wavelet [18]:* The Mexican hat wavelet transform is used to analyze the gait patterns from the acceleration data.
3) *Acc_EigenGait:* The proposed EigenGait algorithm handles the acceleration data.
4) *D_Skeleton [42]:* The position matrix on 20 joints are decomposed by SVD, and the resulting 220-D vectors are used for gait representation.
5) *D_GEV [12]:* The GEV is computed on the human masks extracted from depth data. The PCA is then performed the same way as in our EigenGait for gait features.
6) *D_TrajGait:* The displacement of a trajectory is calculated only on the depth channel, with a codebook size $\mathcal{K} = 1024$.
7) *RGB_TrajGait:* The displacement of a trajectory is calculated on the RGB channels, with $\mathcal{K} = 1024$.
8) *RGBD_TrajGait:* The full TrajGait algorithm, i.e., trajectories extracted from the RGBD channels, with $\mathcal{K} = 1024$.
9) *Acc_EigenGait + RGBD_TrajGait:* The full version of the proposed method by combining EigenGait and TrajGait features. We normalize the EigenGait feature and TrajGait feature independently before concatenating them together. Afterwards, we normalize the concatenated feature as an input data for SVM. The normalization is performed using an $L1$-norm measure.

For clarity, we use Fig. 12(a) and (b) to show the results of the acceleration-based methods and the RGBD-based methods, respectively. In Fig. 12(a), the proposed EigenGait is observed with a clear higher performance than the wavelet-based or FFT-based methods, in handling acceleration data. In Fig. 12(b) we can see that, RGBD_TrajGait obtains an accuracy over 0.90 when using 30% data for training, which is much higher than that of D_Skeleton and D_GEV. The TrajGait has a higher performance on the RGB channels than on the depth channel, which indicates that the color is more effective than the depth in representing gait subdynamics. Meanwhile, RGBD_TrajGait outperforms RGB_TrajGait and D_TrajGait, which simply demonstrates that the color information and depth information can complement each other in

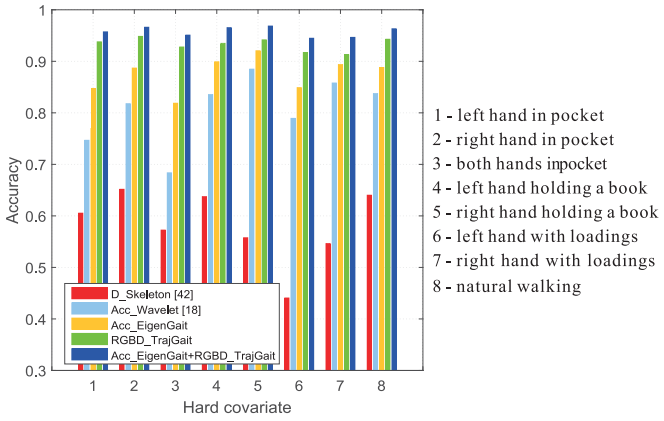

Fig. 13. Classification accuracies under eight hard-covariate conditions using 20% of the data samples for training.

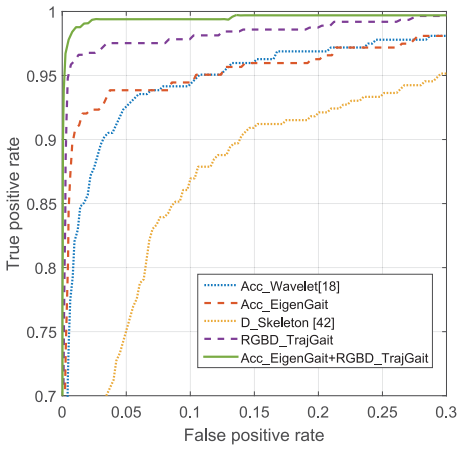

Fig. 14. ROC curves of person identification on dataset #3 using 50% data samples for training.

characterizing the gait. It can also be seen from Fig. 12(b) that, a boosted performance can be achieved by fusing EigenGait (handling acceleration data) and TrajGait (handling RGBD data) features, i.e., EigenGait + TrajGait, which validates the effectiveness of the proposed multisensor data fusion strategy.

C. Robustness

We evaluate the robustness of the proposed method with dataset #3, which contains 2400 data samples of 50 subjects, under eight hard-covariate conditions, as introduced in Section III-B3. Fig. 12(c) shows the results of the proposed method and the comparison methods. We can see that, the TrajGait+EigenGait, the TrajGait, and the EigenGait achieve the top three performances among all the methods. The proposed method, i.e., TrajGait+EigenGait, stably holds a classification accuracy over 0.90 when varying the amount of training data from 10% to 90%, which indicates the proposed method can better handle these hard covariates.

Moreover, we investigate the detailed performance of the proposed method by figuring out the classification accuracies on each kind of hard covariate. As shown in Fig. 13, for EigenGait, the hard covariate "both hands in pocket" leads to the lowest accuracy. It is because that, the acceleration would heavily vary from normal when a person walks with both hands in the pockets. While for TrajGait, "a hand with loadings" will increase the difficulty for gait recognition. This is because the loadings may bring unexpected motions in the color space, as well as in the depth space, e.g., a bag is used to carry the loadings in our case. For the skeleton-based and wavelet-based methods, the average classification accuracy is about 30% and 10% lower than the proposed method, respectively. Comparing with the turbulent performances of the comparison methods on different hard covariates, the proposed method performs rather stably.

D. Person-Identification Performance

Finally, we evaluate the proposed method in the application scenario of person identification, as illustrated by Fig. 1. Half of the data samples in dataset #3 are used for training, and the remaining are used for querying and identification. The average ROC [66], [67] is used as a metric. For each subject, an ROC curve is computed on the results of a one-versus-all binary classification. The ROC curve is created by plotting the true positive rate (TPR) against the false positive rate (FPR) at varying threshold settings. The TPR and FPR are defined by

$$\text{TPR} = \frac{\text{True Positive}}{\text{True Positive} + \text{False Negative}} \tag{12}$$

$$\text{FPR} = \frac{\text{False Positive}}{\text{False Positive} + \text{True Negative}}. \tag{13}$$

Then the average ROC curve is computed based on all ROC curves of 50 subjects. The larger the area under the ROC curve, the better the person-identification performance. The average ROC curves for the proposed method and the comparison methods are plotted in Fig. 14. We can see that, the proposed method by combining EigenGait and TrajGait achieves the best performance. In addition, the EigenGait and the wavelet-based method produce competing performance, but the former achieves higher TPR than the later when the FPR is below 0.05. Thus, the EigenGait would outperform the Wavelet-based method since a lower FPR is often required in a strict identification system. It can also be observed from Fig. 14 that, the TrajGait uniformly outperforms the EigenGait which may simply indicate that the TrajGait features are more discriminative by describing the detailed gait subdynamics.

V. Conclusion

In this paper, the inertia, color and depth sensors were integrated for accurate gait recognition and robust person identification. Specifically, the accelerometer of smartphone and the RGBD sensor of Kinect were employed for data collection. An EigenGait algorithm was proposed to process the acceleration data from inertial sensor in the eigenspace, and capture the general dynamics of the gait. A TrajGait algorithm was proposed to extract gait features on the dense 3-D trajectories from the RGBD data, and capture the more detailed subdynamics. The extracted general dynamics and detailed subdynamics were fused and fed into a linear SVM for training and testing. Datasets collected from 50 subjects were used

for experiments and the results showed the effectiveness of the proposed method against several existing state-of-the-art gait recognition methods.

In the experiments, there are several other interesting findings. First, using the acceleration data, the walking pace has a potential influence on the system accuracy. Uniform walking pace under a normal speed produces better gait recognition than mixed walking paces. Second, using the RGBD data, motion can be better captured by wearing textured clothes, with which we can more accurately infer the detailed gait subdynamics for gait recognition. Third, the proposed construction and encoding of the 3-D dense trajectories can provide more discriminative and robust gait features.

In the future, we plan to further enhance the gait recognition system by configuring more sensors and building more effective classifiers. For example, more Kinects may be installed to capture multiple views of a walking person. For the classifier, other proved techniques in classification, such as the fuzzy-reasoning strategies [68]–[70] may be integrated to improve the recognition accuracy and robustness.

ACKNOWLEDGMENT

The authors would like to thank Z. Zhang, M. Zhou, T. Lei, J. Li, and Y. Wu for doing some experiments in the primary work of this paper.

REFERENCES

[1] M. S. Nixon, T. Tan, and R. Chellapppa, *Human Identification Based on Gait*. New York, NY, USA: Springer, 2006, ch. 1.

[2] J. Zhang, J. Pu, C. Chen, and R. Fleischer, "Low-resolution gait recognition," *IEEE Trans. Syst., Man, Cybern. B, Cybern.*, vol. 40, no. 4, pp. 986–996, Aug. 2010.

[3] M. Ding and G. Fan, "Multilayer joint gait-pose manifolds for human gait motion modeling," *IEEE Trans. Cybern.*, vol. 45, no. 11, pp. 2413–2424, Nov. 2015.

[4] A. Kale, A. N. Rajagopalan, N. Cuntoor, and V. Krueger, "Gait-based recognition of humans using continuous HMMs," in *Proc. Int. Conf. Autom. Face Gesture Recognit.*, Washington, DC, USA, 2002, pp. 336–341.

[5] J. Han and B. Bhanu, "Individual recognition using gait energy image," in *Proc. IEEE Conf. Comput. Vis. Pattern Recognit.*, 2003, pp. 1–8.

[6] Z. Liu and S. Sarkar, "Improved gait recognition by gait dynamics normalization," *IEEE Trans. Pattern Anal. Mach. Intell.*, vol. 28, no. 6, pp. 863–876, Jun. 2006.

[7] Y. Ran, Q. Zheng, R. Chellappa, and T. M. Strat, "Applications of a simple characterization of human gait in surveillance," *IEEE Trans. Syst., Man, Cybern. B, Cybern.*, vol. 40, no. 4, pp. 1009–1020, Aug. 2010.

[8] J. Gu, X. Ding, S. Wang, and Y. Wu, "Action and gait recognition from recovered 3-D human joints," *IEEE Trans. Syst., Man, Cybern. B, Cybern.*, vol. 40, no. 4, pp. 1021–1033, Aug. 2010.

[9] W. Kusakunniran, Q. Wu, J. Zhang, Y. Ma, and H. Li, "A new view-invariant feature for cross-view gait recognition," *IEEE Trans. Inf. Forensics Security*, vol. 8, no. 10, pp. 1642–1653, Oct. 2013.

[10] N. V. Boulgouris and X. Huang, "Gait recognition using HMMs and dual discriminative observations for sub-dynamics analysis," *IEEE Trans. Image Process.*, vol. 22, no. 9, pp. 3636–3647, Sep. 2013.

[11] M. Goffredo, I. Bouchrika, J. N. Carter, and M. S. Nixon, "Self-calibrating view-invariant gait biometrics," *IEEE Trans. Syst., Man, Cybern. B, Cybern.*, vol. 40, no. 4, pp. 997–1008, Aug. 2010.

[12] S. Sivapalan, D. Chen, S. Denman, S. Sridharan, and C. Fookes, "Gait energy volumes and frontal gait recognition using depth images," in *Proc. Int. Joint Conf. Biometrics*, Washington, DC, USA, 2011, pp. 1–6.

[13] V. John, G. Englebienne, and B. Krose, "Person re-identification using height-based gait in colour depth camera," in *Proc. Int. Conf. Image Process.*, Melbourne, VIC, Australia, 2013, pp. 3345–3349.

[14] P. Chattopadhyay, A. Roy, S. Sural, and J. Mukhopadhyay, "Pose depth volume extraction from RGB-D streams for frontal gait recognition," *J. Vis. Commun. Image Representation*, vol. 25, no. 1, pp. 53–63, 2014.

[15] J. Mantyjarvi, M. Lindholm, E. Vildjiounaite, S.-M. Makela, and H. A. Ailisto, "Identifying users of portable devices from gait pattern with accelerometers," in *Proc. IEEE Conf. Acoustics Speech Signal Process.*, Philadelphia, PA, USA, 2005, pp. 973–976.

[16] L. Rong, D. Zhiguo, Z. Jianzhong, and L. Ming, "Identification of individual walking patterns using gait acceleration," in *Proc. Int. Conf. Bioinformat. Biomed. Eng.*, Wuhan, China, 2007, pp. 543–546.

[17] J. R. Kwapisz, G. M. Weiss, and S. A. Moore, "Cell phone-based biometric identification," in *Proc. Int. Conf. Biometrics Theory Appl. Syst.*, Washington, DC, USA, 2010, pp. 1–7.

[18] F. Juefei-Xu, C. Bhagavatula, A. Jaech, U. Prasad, and M. Savvides, "Gait-ID on the move: Pace independent human identification using cell phone accelerometer dynamics," in *Proc. Int. Conf. Biometrics Theory Appl. Syst.*, Arlington County, VA, USA, 2012, pp. 8–15.

[19] N. T. Trung *et al.*, "Phase registration in a gallery improving gait authentication," in *Proc. Int. Joint Conf. Biometrics*, Washington, DC, USA, 2011, pp. 1–7.

[20] N. T. Trung, Y. Makihara, H. Nagahara, Y. Mukaigawa, and Y. Yagi, "Performance evaluation of gait recognition using the largest inertial sensor-based gait database," in *Proc. IAPR Int. Conf. Biometrics*, New Delhi, India, 2012, pp. 360–366.

[21] B. Sun, Y. Wang, and J. Banda, "Gait characteristic analysis and identification based on the iPhone's accelerometer and gyrometer," *Sensors*, vol. 14, no. 9, pp. 17037–17054, 2014.

[22] J. E. Cutting and L. T. Kozlowski, "Recognition of friends by their walk," *Bull. Psychonomic Soc.*, vol. 9, no. 5, pp. 353–356, 1977.

[23] A. M. de-la Herran, B. Garcia-Zapirain, and A. Mendez-Zorrilla, "Gait analysis methods: An overview of wearable and non-wearable systems, highlighting clinical applications," *Sensors*, vol. 14, no. 2, pp. 3362–3394, 2014.

[24] C. BenAbdelkader, R. Cutler, and L. Davis, "Stride and cadence as a biometric in automatic person identification and verification," in *Proc. Int. Conf. Autom. Face Gesture Recognit.*, Washington, DC, USA, 2002, pp. 372–377.

[25] L. Wang, T. Tan, H. Ning, and W. Hu, "Silhouette analysis-based gait recognition for human identification," *IEEE Trans. Pattern Anal. Mach. Intell.*, vol. 25, no. 12, pp. 1505–1518, Dec. 2003.

[26] A. Kale *et al.*, "Identification of humans using gait," *IEEE Trans. Image Process.*, vol. 13, no. 9, pp. 1163–1173, Sep. 2004.

[27] D. Tao, X. Li, X. Wu, and S. J. Maybank, "General tensor discriminant analysis and Gabor features for gait recognition," *IEEE Trans. Pattern Anal. Mach. Intell.*, vol. 29, no. 10, pp. 1700–1715, Oct. 2007.

[28] L. Wang, H. Z. Ning, T. N. Tan, and W. M. Hu, "Fusion of static and dynamic body biometrics for gait recognition," in *Proc. Int. Conf. Comput. Vis.*, Nice, France, 2003, pp. 1449–1454.

[29] D. Tolliver and R. T. Collins, "Gait shape estimation for identification," in *Proc. Audio Video Based Biometric Person Authentication*, Guildford, U.K., 2003, pp. 734–742.

[30] J. Han and B. Bhanu, "Statistical feature fusion for gait-based human recognition," in *Proc. IEEE Conf. Comput. Vis. Pattern Recognit.*, Washington, DC, USA, 2004, pp. II-842–II-847.

[31] Z. Zhang and N. F. Troje, "View-independent person identification from human gait," *Neurocomputing*, vol. 69, nos. 1–3, pp. 250–256, 2005.

[32] C. BenAbdelkader, R. Culter, H. Nanda, and L. Davis, "EigenGait: Motion-based recognition of people using image self-similarity," in *Proc. Int. Conf. Audio Video Based Pers. Authentication*, Halmstad, Sweden, 2001, pp. 284–294.

[33] C. Chen, J. Liang, and X. Zhu, "Gait recognition based on improved dynamic Bayesian networks," *Pattern Recognit.*, vol. 44, no. 4, pp. 988–995, 2011.

[34] I. Venkat and P. De Wilde, "Robust gait recognition by learning and exploiting sub-gait characteristics," *Int. J. Comput. Vis.*, vol. 91, no. 1, pp. 7–23, 2011.

[35] M. Hu, Y. Wang, Z. Zhang, D. Zhang, and J. J. Little, "Incremental learning for video-based gait recognition with LBP flow," *IEEE Trans. Cybern.*, vol. 43, no. 1, pp. 77–89, Feb. 2013.

[36] T. H. Lam, K. H. Cheung, and J. N. K. Liu, "Gait flow image: A silhouette-based gait representation for human identification," *Pattern Recognit.*, vol. 44, no. 4, pp. 973–987, 2011.

[37] F. M. Castro, M. J. Marin-Jimenez, and R. Medina-Carnicer, "Pyramidal fisher motion for multiview gait recognition," in *Proc. Int. Conf. Pattern Recognit.*, Stockholm, Sweden, 2014, pp. 1692–1697.

[38] W. Kusakunniran, "Attribute-based learning for gait recognition using spatio-temporal interest points," *Image Vis. Comput.*, vol. 32, no. 12, pp. 1117–1126, 2014.
[39] C. Yam, M. S. Nixon, and J. N. Carter, "Gait recognition by walking and running: A model-based approach," in *Proc. Asian Conf. Comput. Vis.*, Melbourne, VIC, Australia, 2002, pp. 1–6.
[40] D. Cunado, M. S. Nixon, and J. N. Carter, "Automatic extraction and description of human gait models for recognition purposes," *Comput. Vis. Image Understanding*, vol. 90, no. 1, pp. 1–41, 2003.
[41] P. F. Felzenszwalb, R. B. Girshick, D. McAllester, and D. Ramanan, "Object detection with discriminatively trained part-based models," *IEEE Trans. Pattern Anal. Mach. Intell.*, vol. 32, no. 9, pp. 1627–1645, Sep. 2010.
[42] B. C. Munsell, A. Temlyakov, C. Qu, and S. Wang, "Person identification using full-body motion and anthropometric biometrics from kinect videos," in *Proc. Eur. Conf. Comput. Vis. Workshop*, Florence, Italy, 2012, pp. 91–100.
[43] M. Gabel, R. Gilad-Bachrach, E. Renshaw, and A. Schuster, "Full body gait analysis with kinect," in *Proc. Int. Conf. IEEE Eng. Med. Biol. Soc.*, 2012, pp. 1964–1967.
[44] L. Igual, À. Lapedriza, and R. Borràs, "Robust gait-based gender classification using depth cameras," *EURASIP J. Image Video Process.*, vol. 2013, no. 1, pp. 1–11, 2013.
[45] P. Chattopadhyay, S. Sural, and J. Mukherjee, "Frontal gait recognition from incomplete sequences using RGB-D camera," *IEEE Trans. Inf. Forensics Security*, vol. 9, no. 11, pp. 1843–1856, Nov. 2014.
[46] M. O. Derawi, P. Bours, and K. Holien, "Improved cycle detection for accelerometer based gait authentication," in *Proc. Int. Conf. Intell. Inf. Hiding Multimedia Signal Process.*, Darmstadt, Germany, 2010, pp. 312–317.
[47] D. Gafurov, E. Snekkenes, and P. Bours, "Improved gait recognition performance using cycle matching," in *Proc. Int. Conf. Adv. Inf. Netw. Appl.*, 2010, pp. 836–841.
[48] H. K. Y. Chan *et al.*, "Feasibility study on iPhone accelerometer for gait detection," in *Proc. Int. Conf. Pervasive Comput. Technol. Healthcare (PervasiveHealth)*, Dublin, Ireland, 2011, pp. 184–187.
[49] T. T. Ngo, Y. Makihara, H. Nagahara, Y. Mukaigawa, and Y. Yagi, "The largest inertial sensor-based gait database and performance evaluation of gait-based personal authentication," *Pattern Recognit.*, vol. 47, no. 1, pp. 228–237, 2014.
[50] Y. Zhang *et al.*, "Accelerometer-based gait recognition by sparse representation of signature points with clusters," *IEEE Trans. Cybern.*, vol. 45, no. 9, pp. 1864–1875, Sep. 2015.
[51] T. Kobayashi and N. Otsu, "Action and simultaneous multiple-person identification using cubic higher-order local auto-correlation," in *Proc. Int. Conf. Pattern Recognit.*, Cambridge, U.K., 2004, pp. 741–744.
[52] N. Gkalelis, A. Tefas, and I. Pitas, "Human identification from human movements," in *Proc. IEEE Int. Conf. Image Process.*, Cairo, Egypt, 2009, pp. 2585–2588.
[53] A. Iosifidis, A. Tefas, and I. Pitas, "Activity-based person identification using fuzzy representation and discriminant learning," *IEEE Trans. Inf. Forensics Security*, vol. 7, no. 2, pp. 530–542, Apr. 2012.
[54] A. Iosifidis, A. Tefas, and I. Pitas, "Person identification from actions based on dynemes and discriminant learning," in *Proc. IEEE Int. Workshop Biometrics Forensics*, Lisbon, Portugal, 2013, pp. 1–4.
[55] J. Lu, J. Hu, X. Zhou, and Y. Shang, "Activity-based person identification using sparse coding and discriminative metric learning," in *Proc. ACM Int. Conf. Multimedia*, Nara, Japan, 2012, pp. 1061–1064.
[56] H. Yan, J. Lu, and X. Zhou, "Activity-based person identification using discriminative sparse projections and orthogonal ensemble metric learning," in *Proc. Eur. Conf. Comput. Vis. Workshops*, Zürich, Switzerland, 2014, pp. 809–824.
[57] H. Yan, "Discriminative sparse projections for activity-based person recognition," *Neurocomputing*, vol. 208, pp. 183–192, Oct. 2016.
[58] J. Wu, J. Konrad, and P. Ishwar, "The value of multiple viewpoints in gesture-based user authentication," in *Proc. IEEE Conf. Comput. Vis. Pattern Recognit. Workshops*, Columbus, OH, USA, 2014, pp. 90–97.
[59] I. Kviatkovsky, I. Shimshoni, and E. Rivlin, "Person identification from action styles," in *Proc. IEEE Conf. Comput. Vis. Pattern Recognit. Workshops*, Boston, MA, USA, 2015, pp. 84–92.
[60] M. Turk and A. Pentland, "Eigenfaces for recognition," *J. Cogn. Neurosci.*, vol. 3, no. 1, pp. 71–86, 1991.
[61] G. Farnebäck, "Two-frame motion estimation based on polynomial expansion," in *Scandinavian Conference on Image Analysis*, Halmstad, Sweden: Springer, 2003, pp. 363–370.
[62] J. Shotton *et al.*, "Efficient human pose estimation from single depth images," *IEEE Trans. Pattern Anal. Mach. Intell.*, vol. 35, no. 12, pp. 2821–2840, Dec. 2012.
[63] H. Wang, A. Kläser, C. Schmid, and C.-L. Liu, "Action recognition by dense trajectories," in *Proc. IEEE Conf. Comput. Vis. Pattern Recognit.*, Colorado Springs, CO, USA, 2011, pp. 3169–3176.
[64] W. Kusakunniran, Q. Wu, J. Zhang, and H. Li, "Gait recognition across various walking speeds using higher order shape configuration based on a differential composition model," *IEEE Trans. Syst., Man, Cybern. B, Cybern.*, vol. 42, no. 6, pp. 1654–1668, Dec. 2012.
[65] C.-C. Chang and C.-J. Lin, "LIBSVM: A library for support vector machines," *ACM Trans. Intell. Syst. Technol.*, vol. 2, no. 3, 2011, Art. no. 27.
[66] T. Fawcett, "An introduction to ROC analysis," *Pattern Recognit. Lett.*, vol. 27, no. 8, pp. 861–874, 2006.
[67] Q. Zou, Y. Cao, Q. Li, C. Huang, and S. Wang, "Chronological classification of ancient paintings using appearance and shape features," *Pattern Recognit. Lett.*, vol. 49, pp. 146–154, Nov. 2014.
[68] Q. Liang and J. M. Mendel, "Interval type-2 fuzzy logic systems: Theory and design," *IEEE Trans. Fuzzy Syst.*, vol. 8, no. 5, pp. 535–550, Oct. 2000.
[69] H. Li, Y. Gao, P. Shi, and H.-K. Lam, "Observer-based fault detection for nonlinear systems with sensor fault and limited communication capacity," *IEEE Trans. Autom. Control*, vol. 61, no. 9, pp. 2745–2751, Sep. 2015.
[70] H. Li, C. Wu, S. Yin, and H.-K. Lam, "Observer-based fuzzy control for nonlinear networked systems under unmeasurable premise variables," *IEEE Trans. Fuzzy Syst.*, vol. 24, no. 5, pp. 1233–1245, Oct. 2016.

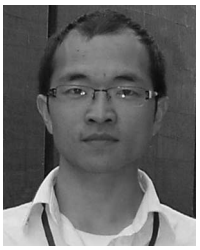

Qin Zou (M'13) received the B.E. degree in information science and the Ph.D. degree in photogrammetry and remote sensing (computer vision) from Wuhan University, Wuhan, China, in 2004 and 2012, respectively.

He was a visiting student with the Computer Vision Laboratory, University of South Carolina, Columbia, SC, USA, from 2010 to 2011. He is currently an Assistant Professor with the School of Computer Science, Wuhan University. His current research interests include computer vision, machine learning, and multimedia processing.

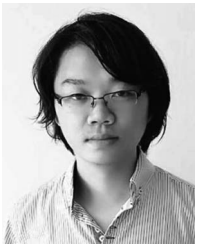

Lihao Ni received the B.S. degree in computer science from Wuhan University, Wuhan, China, in 2016, where he is currently pursuing the master's degree with the School of Computer Science.

His current research interests include pattern recognition and biometric identification.

Mr. Ni was a recipient of the First Prize in the College Group of the "National Internet of Things Competition, China," in 2015.

Qian Wang (M'12) received the B.S. degree from Wuhan University, Wuhan, China, in 2003, the M.S. degree from the Shanghai Institute of Microsystem and Information Technology, Chinese Academy of Sciences, Beijing, China, in 2006, and the Ph.D. degree from the Illinois Institute of Technology, Chicago, IL, USA, in 2012, all in electrical engineering.

He is currently a Professor with the School of Computer Science, Wuhan University. His current research interests include wireless network security and privacy, cloud computing security, and applied cryptography.

Dr. Wang was a co-recipient of the Best Paper Award from the IEEE ICNP 2011. He is an expert under "1000 Young Talents Program" of China. He is a member of ACM.

Qingquan Li received the Ph.D. degree in GIS and photogrammetry from the Wuhan Technical University of Surveying and Mapping, Wuhan, China, in 1998.

He was an Assistant Professor with Wuhan University, from 1988 to 1996, where he became an Associate Professor in 1996 and has been a Professor since 1998. He is currently a Professor with the State Key Laboratory of Information Engineering in Surveying, Mapping and Remote Sensing, Wuhan University, and the President and a Professor with Shenzhen University, Shenzhen, China, where he is the Director of the Shenzhen Key Laboratory of Spatial Smart Sensing and Service. His current research interests include intelligent transportation systems, 3-D and dynamic data modeling, location-based service, and multisensor integration.

Dr. Li is an Academician of the International Academy of Sciences for Europe and Asia, an expert in Modern Traffic with the National 863 Plan, and an Editorial Board Member of the *Surveying and Mapping Journal* and the *Wuhan University Journal (Information Science Edition)*.

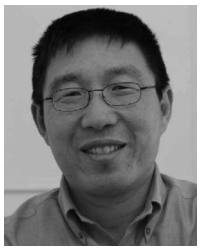

Song Wang (M'02–SM'13) received the Ph.D. degree in electrical and computer engineering from the University of Illinois at Urbana–Champaign (UIUC), Champaign, IL, USA, in 2002.

He was a Research Assistant with the Image Formation and Processing Group, Beckman Institute, UIUC, from 1998 to 2002. In 2002, he joined the Department of Computer Science and Engineering, University of South Carolina, Columbia, SC, USA, where he is currently a Professor. His current research interests include computer vision, medical image processing, and machine learning.

Dr. Wang is currently serving as the Publicity/Web Portal Chair of the Technical Committee of Pattern Analysis and Machine Intelligence of the IEEE Computer Society, and an Associate Editor of *Pattern Recognition Letters*. He is a Senior Member of the IEEE Computer Society.